

Long-time evolution of pulses in the Korteweg-de Vries equation in the absence of solitons revisited: Whitham method

M. Isoard,¹ A. M. Kamchatnov,^{2,3} and N. Pavloff¹

¹*LPTMS, CNRS, Univ. Paris-Sud, Université Paris-Saclay, 91405 Orsay, France*

²*Institute of Spectroscopy, Russian Academy of Sciences, Troitsk, Moscow, 108840, Russia*

³*Moscow Institute of Physics and Technology, Institutsky lane 9, Dolgoprudny, Moscow region, 141701, Russia*

We consider the long-time evolution of pulses in the Korteweg-de Vries equation theory for initial distributions which produce no soliton, but instead lead to the formation of a dispersive shock wave and of a rarefaction wave. An approach based on Whitham modulation theory makes it possible to obtain an analytic description of the structure and to describe its self-similar behavior near the soliton edge of the shock. The results are compared with numerical simulations.

I. INTRODUCTION

It is well known that pulses propagating through a nonlinear medium typically experience wave breaking. Their long time evolution depends on which effect—in addition to the nonlinearity—dominates after the wave breaking moment: viscosity or dispersion. If viscosity dominates, then the shock corresponds to a region of localized extend in which the slow variables display a sharp transition. A typical small-amplitude viscous shock can be modeled by the Burgers equation

$$u_t + uu_x = \nu u_{xx}, \quad (1)$$

for which a full analytic theory has been developed (see, e.g., Ref. [1]). For a positive initial profile $u(x, t = 0) \equiv u_0(x) > 0$ which is well enough localized (i.e., $u_0(x) \rightarrow 0$ fast enough for $|x| \rightarrow \infty$) the time-evolved pulse acquires a triangle-like shape at its front edge (or at its rear edge if $u_0(x) < 0$ [38]) gradually spreading out with decreasing amplitude.

The situation changes drastically if dispersive effects dominate rather than viscosity. In this case the typical evolution can be described by the celebrated Korteweg-de Vries (KdV) equation

$$u_t + 6uu_x + u_{xxx} = 0, \quad (2)$$

which admits oscillating solutions ranging from linear waves to bright solitons. A positive localized initial pulse $u_0(x) > 0$, after an intermediate stage of wave breaking and complicated deformation, eventually evolves into a sequence of solitons with some amount of linear dispersive waves. The characteristics of the solitons are determined by the initial distribution $u_0(x)$. If this initial pulse is intense enough—so that the number of solitons is large—one may use for determining the parameters of these solitons the asymptotic formula of Karpman [2] obtained in the framework of the inverse scattering transform method discovered by Gardner, Green, Kruskal and Miura [3]. However, if $u_0(x) < 0$, since Eq. (2) does not admit dark (i.e., “negative”) soliton, wave breaking does not result in the formation of solitons in the asymptotic regime $t \rightarrow \infty$, but it rather leads to the formation of a dispersive shock wave (DSW) connected to a triangle-like rarefaction wave which is the remnant of the initial

trough. The shape and the time evolution of this oscillatory structure is highly nontrivial and considerable efforts have been invested into its study.

In an early investigation of Berezin and Karpman [4] it was shown that the KdV equation admits solutions of the form

$$u(x, t) = \frac{1}{t^{2/3}} f\left(\frac{x}{t^{1/3}}\right), \quad (3)$$

and numerical simulations of these authors demonstrated that some region of the evolving wave structure is indeed described by solutions of type (3). The existence of such a region was confirmed by the inverse scattering transform method in Refs. [5, 6] and its “quasi-linear” part was studied in Ref. [7]. An extensive study of the asymptotic evolution of the pulse in the absence of solitons was performed in Ref. [8] where different characteristic parts of the wave structure were distinguished and their main parameters were calculated. However, in this reference, Ablowitz and Segur—who first explicitly point to the formation of a dispersive shock wave—confined themselves to the analytic study of typical limiting cases and explicit formulae for the whole dispersive shock wave region were found much later [9] with the use of a quite involved analysis of the associated Riemann-Hilbert problem. This approach was developed further in Refs. [10–12] and other papers.

Although the above mentioned approaches are mathematically strict, the methods used are difficult and the theory developed has not found applications to concrete problems related with other integrable evolution equations. Since the question of evolution of pulses in the absence of solitons is related with experiments in physics of water waves [13, 14], Bose-Einstein condensates [15, 16] and nonlinear optics [17, 18], the development of a simpler and more transparent physically approach is desirable. Such an approach, based on the Whitham theory of modulations of nonlinear waves [19], was suggested long ago by Gurevich and Pitaevskii [20] and since that time it has developed into a powerful method with numerous applications (see, e.g., the review article [21]). Despite the facts that some elements of the Whitham theory were used in Refs. [6, 8] and that the general solution of the solitonless initial value problem has been

obtained in Ref. [22], no asymptotic analysis has been performed within Whitham's formalism, so that its relationship with the previous results remained unclear.

The main goal of the present paper is to fill this gap and to apply the Whitham theory to the description of the asymptotic evolution of initial pulses in the small dispersion limit (or for wide pulses) under the condition of absence of solitons. We show that the combination of two ideas—self-similarity of the solution and quasi-simple character [23] of the dispersive shock wave—permits a asymptotic analysis of the solution. The relatively simple theory developed in the present work should be useful in the analysis of experiments devoted to the evolution of pulses of this type.

The paper is organized as follows. In Sec. II we present the main aspects of Whitham theory and of the generalized hodograph method applying to quasi-simple waves (following Refs. [22–28]). In Sec. III the application of the ideas of Ref. [23] to the soliton edge of the DSW makes it possible to find the law of motion of this edge and suggests its self-similar asymptotic behavior consistent with Eq. (3). In Sec. IV we perform the large time asymptotic analysis of the rear (soliton) part of the dispersive shock wave by the Whitham method within the self-similarity assumption. This yields a surprisingly simple derivation of the solution of Ref. [9]. The description of the DSW in its full range by the method of El and Khodorovskii [22] is presented in a self-contained manner in Sec. V. In this section we consider the time evolution of several initial profiles illustrating the possible different behaviors in the shock region and compare the theoretical results with numerical simulations. We present our conclusions in Sec. VI.

II. WHITHAM THEORY AND THE GENERALIZED HODOGRAPH METHOD

A. The smooth part of the profile

We consider an initial pulse with non-positive profile $u(x, t = 0) = u_0(x)$ defined on finite interval of x and having a single minimum $\min_{x \in \mathbb{R}} \{u_0(x)\} = -1$ (this value can be changed by an appropriate re-scaling on u , x and t). The initial profile is assumed to be smooth (i.e., for finite pulses with the length x_0 we assume $x_0 \gg 1$), so that in a first stage of evolution one can neglect dispersive effects. This amounts to replace the KdV dynamics by the Hopf equation

$$r_t + 6 r r_x = 0. \quad (4)$$

We change notation here to mark the difference between $r(x, t)$, solution of (4), and $u(x, t)$ which is the global solution of the KdV equation (2).

The solution of the Hopf equation is well known and it is given in implicit form in terms of functions inverse to $u_0(x)$. In the case we consider $u_0(x)$ has a single minimum and the inverse function is two-valued. We denote

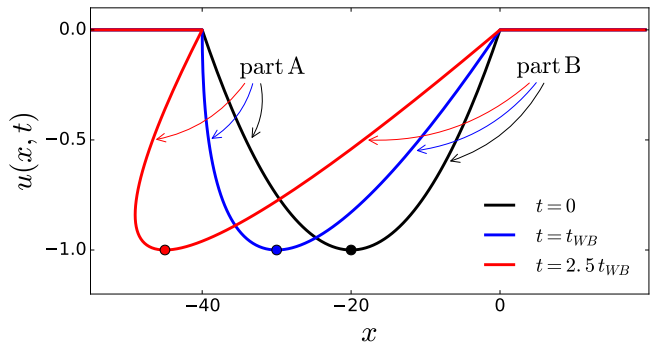


FIG. 1: Dispersionless evolution of the initial parabolic profile (6) with $x_0 = 40$. The black, blue and red solid lines represent $r(x, t)$ solution of (4) for times $t = 0$, $t = t_{WB}$ and $t = 2.5 t_{WB}$. The dots represent the position of the minimum $\min_{x \in \mathbb{R}} \{r(x, t)\}$ which separates parts A (at the left) and B (at the right) of the profile.

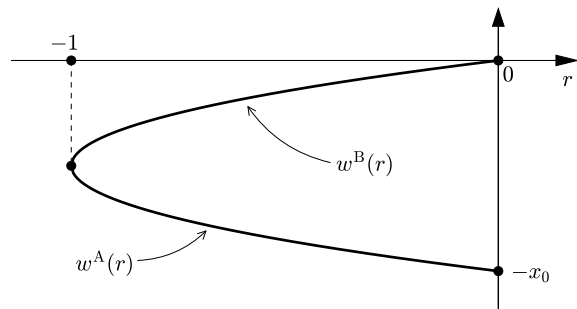


FIG. 2: The two branches $w^A(r)$ and $w^B(r)$ of the reciprocal function of $u_0(x)$. The figure is drawn for the initial parabolic profile (6) (the corresponding expressions of $w^A(r)$ and $w^B(r)$ are given in Eq. (7)) but the behavior is the generic one.

its two branches as $w^A(r)$ and $w^B(r)$, where the first function refers to the part of the pulse to the left of its minimum and the second one to its right. Then the solution of the Hopf equation is given by the formulae

$$x - 6 r t = w^A(r), \quad (5a)$$

$$x - 6 r t = w^B(r). \quad (5b)$$

For example, in case of a parabolic initial pulse

$$u_0(x) = \begin{cases} 4x(x+x_0)/x_0^2 & \text{for } -x_0 \leq x \leq 0, \\ 0 & \text{elsewhere,} \end{cases} \quad (6)$$

the inverse functions are equal to

$$\begin{cases} w^A(r) = \frac{x_0}{2} (-1 - \sqrt{1+r}), \\ w^B(r) = \frac{x_0}{2} (-1 + \sqrt{1+r}), \end{cases} \quad \text{where } r \in [-1, 0]. \quad (7)$$

Figure (1) represents the initial profile (6) and its time evolution as computed from Eqs. (5), i.e., without taking dispersive effects into account. Figure (2) represents

the corresponding functions $w^A(r)$ and $w^B(r)$. In the following we shall illustrate the explicit computations by this simple initial profile. Other types of profiles, with less generic behaviors, will be presented and discussed in Sec. V.

The wave breaking time is the time $t_{\text{WB}} = 1/\max(-6 du_0/dx)$ at which the solution of (4) becomes infinitely steep (see, e.g., Ref. [1]). In the present work we consider initial profiles for which the largest slope $\max(-du_0/dx)$ is reached at $x = -x_0$ for $r = 0$ and thus

$$t_{\text{WB}} = -\frac{1}{6} \left(\frac{dw^A}{dr} \right)_{r=0}. \quad (8)$$

For the initial profile (6) we get $t_{\text{WB}} = x_0/24$. For $t \geq t_{\text{WB}}$ the dispersionless approximation fails (the corresponding formal solution of the Hopf equation is multi-valued), and a DSW is formed, initially around $x = -x_0$, which then propagates in the negative x direction. We now explain how it can be described within Whitham modulational theory.

B. Periodic solutions and their modulations

The KdV equation (2) admits nonlinear periodic solutions which can be written in terms of three parameters $r_1 \leq r_2 \leq r_3$ as (see, e.g., [29])

$$u(x, t) = r_3 + r_2 - r_1 - 2(r_2 - r_1) \times \text{sn}^2(\sqrt{r_3 - r_1}(x - Vt), m), \quad (9)$$

$$\text{where } V = 2(r_1 + r_2 + r_3), \quad \text{and } m = \frac{r_2 - r_1}{r_3 - r_1}.$$

The notation “sn” in the above formula refers to the Jacobi sine function (see, e.g., Ref. [30]). For constant parameters r_i expression (9) is an exact (single phase) solution of the KdV equation, periodic in time and space with wavelength

$$L = \frac{2K(m)}{\sqrt{r_3 - r_1}}, \quad (10)$$

where $K(m)$ is the complete elliptic integral of the first kind.

According to the Gurevich-Pitaevskii scheme, a DSW may be described as a modulated nonlinear periodic wave of type (9) for which the r_i 's slowly depend on time and position and evolve according to the Whitham equations (see, e.g, Refs. [21, 29])

$$\partial_t r_i + v_i(r_1, r_2, r_3) \partial_x r_i = 0, \quad i = 1, 2, 3. \quad (11)$$

The quantities v_i in these equations are the Whitham velocities. Their explicit expressions have first been derived by Whitham [19], and can also be obtained from the relation

$$v_i = \left(1 - \frac{L}{\partial_i L} \partial_i \right) L = V - 2 \frac{L}{\partial_i L}, \quad (12)$$

where L is the wavelength (10) of the nonlinear periodic solution (9) and ∂_i stands for ∂_{r_i} . One gets

$$\begin{aligned} v_1 &= 2(r_1 + r_2 + r_3) + \frac{4(r_2 - r_1)K(m)}{E(m) - K(m)}, \\ v_2 &= 2(r_1 + r_2 + r_3) - \frac{4(r_2 - r_1)(1 - m)K(m)}{E(m) - (1 - m)K(m)}, \\ v_3 &= 2(r_1 + r_2 + r_3) + \frac{4(r_3 - r_1)(1 - m)K(m)}{E(m)}, \end{aligned} \quad (13)$$

where $E(m)$ is the complete elliptic integral of the second kind.

Since Eqs. (11) have a diagonal form (that is, they include derivatives of a single parameter r_i in each equation), the variables r_i are called Riemann invariants of the Whitham equations—Riemann was the first who introduced such variables in the theory of nonlinear waves.

The two edges of the DSW are denoted as $x_L(t)$ and $x_R(t)$. The first one is the small amplitude edge, it is at the left of the DSW in the case we consider. Within Whitham approximation, it makes contact between the DSW and the undisturbed profile: $u(x, t) = 0$ for $x \leq x_L(t)$. The small amplitude version of (9) corresponds to the limit $m \ll 1$ and takes the form

$$u(x, t) = r_3 + (r_2 - r_1) \cos[2\sqrt{r_3 - r_1}(x - Vt)]. \quad (14)$$

In this harmonic linear limit, $r_2 \rightarrow r_1$ ($m \rightarrow 0$) and the Whitham velocities (13) reduce to

$$\begin{aligned} v_1|_{r_2=r_1} &= v_2|_{r_2=r_1} = 12r_1 - 6r_3, \\ v_3|_{r_2=r_1} &= 6r_3. \end{aligned} \quad (15)$$

Around the left boundary of the DSW, the amplitude $2(r_2 - r_1)$ of the oscillations is small and since this edge propagates along a zero background, we arrive at the conclusion that $r_3 = 0$ and $r_1 = r_2$ for $x = x_L(t)$.

The other edge, at the right side of the DSW, is the large amplitude soliton edge, with $m = 1$. Therefore we must have here $r_2 = r_3$ and in this limit the nonlinear pattern (9) degenerates into a soliton solution of the form

$$u(x, t) = r_1 + \frac{2(r_2 - r_1)}{\cosh^2[\sqrt{r_2 - r_1}(x - Vt)]}. \quad (16)$$

This implies that the right of the DSW is bounded by a soliton for which the Whitham velocities are given by

$$\begin{aligned} v_1|_{r_2=r_3} &= 6r_1, \\ v_2|_{r_2=r_3} &= v_3|_{r_2=r_3} = 2r_1 + 4r_3. \end{aligned} \quad (17)$$

The contact of the DSW with the smooth profile (which prevails for $x \geq x_R(t)$) imposes the condition $r_1(x_R(t), t) = r(x_R(t), t)$, where $r(x, t)$ is a solution of the Hopf equation (4) with initially $r(x, 0) = u_0(x)$.

Therefore the description of the DSW for $x \in [x_L(t), x_R(t)]$ is consistent with a constant value $r_3(x, t) =$

0 for the larger Riemann parameter, while the two others satisfy the boundary conditions

$$r_1(x_R(t), t) = r(x_R(t), t) \equiv r_R(t), \quad (18a)$$

$$r_2(x_R(t), t) = 0,$$

$$r_1(x_L(t), t) = r_2(x_L(t), t) \equiv r_L(t). \quad (18b)$$

Note that all the above functions are only defined after the wave breaking time, i.e., for $t \geq t_{WB}$.

C. Generalized hodograph method

As just discussed, for the type of structure we aim at describing, two Riemann invariants (r_1 and r_2) change along the DSW. The corresponding shock is thus not a simple wave solution corresponding to a step-like initial profile; it belongs to the class of “quasi-simple waves” introduced in Ref. [23]. In this case, Eq. (11) with $i = 3$ is trivially satisfied (by $r_3 = 0$) and for solving the remaining two Whitham equations we use the so-called generalized hodograph method of Tsarev [31]. To this end, one introduces two functions $W_i(r_1, r_2)$ ($i = 1$ or 2) making it possible to write a vector generalization of Eq. (5) for the Whitham system

$$x - v_i(r_1, r_2)t = W_i(r_1, r_2), \quad i = 1, 2. \quad (19)$$

For the sake of brevity we have noted in the above equation $v_i(r_1, r_2) = v_i(r_1, r_2, r_3 = 0)$ for $i \in \{1, 2\}$; we will keep this notation henceforth. The W_i 's must satisfy the compatibility equation found by substituting (19) into (11). This leads to the Tsarev equations:

$$\frac{\partial_j W_i}{W_i - W_j} = \frac{\partial_j v_i}{v_i - v_j}, \quad \text{for } i \neq j. \quad (20)$$

One can show (see, e.g., [25, 27, 28]) that (20) is solved for W_i 's of the form

$$W_i = \left(1 - \frac{L}{\partial_i L} \partial_i\right) \mathcal{W} = \mathcal{W} + \left(\frac{1}{2}v_i - r_1 - r_2\right) \partial_i \mathcal{W}, \quad (21)$$

where $\mathcal{W}(r_1, r_2)$ is solution of the Euler-Poisson equation

$$\partial_{12} \mathcal{W} = \frac{\partial_1 \mathcal{W} - \partial_2 \mathcal{W}}{2(r_1 - r_2)}. \quad (22)$$

There is however a subtle point here, which was first understood in Ref. [23] (see also Ref. [22]): after the wave breaking time, the development of the dispersive shock wave occurs in *two* steps. Initially (when t is close to t_{WB}), the DSW is connected at its right edge to the smooth profile coming from the time evolution of part A of the initial profile. We denote this as case “A” which occurs in “region A” of the (x, t) plane. Then, after a while, the left part of the initial profile (part A) has been “swallowed” by the DSW which is then connected to the smooth profile coming from the time evolution of part B of $u_0(x)$

(this is case “B”, “region B” of the (x, t) plane). In case A, for a given time t , the lower value of $u(x, t)$ is reached within the smooth part of the profile and keeps its initial values (-1). In case B, the minimum $\min_{x \in \mathbb{R}} \{u(x, t)\}$ is reached inside the DSW (or at its boundary), is negative and larger than -1 (i.e., less pronounced than in case A) and asymptotically tends to 0 for large time.

In region A of the (x, t) plane, we denote by $\mathcal{W}^A(r_1, r_2)$ the solution of the Euler-Poisson equation, in region B we denote it instead as $\mathcal{W}^B(r_1, r_2)$. These two forms are joined by the line $r_1 = -1$ (cf. the upper left plot of Fig. 5) where

$$\mathcal{W}^A(-1, r_2) = \mathcal{W}^B(-1, r_2). \quad (23)$$

Since the general solution of the Euler-Poisson equation with the appropriate boundary conditions, and the construction of the resulting nonlinear pattern are quite involved, we shall first consider some particular—but useful—results which follow from general principles of the Whitham theory.

III. MOTION OF THE SOLITON EDGE OF THE SHOCK

During the first stage of evolution of the DSW, its right (solitonic) edge is connected to the smooth dispersionless solution described by formula (5a), that is we have here

$$x_R - 6r_R t = w^A(r_R). \quad (24)$$

On the other hand, in vicinity of this boundary the Whitham equations (11) with the limiting expressions (17) (where $r_3 = 0$) for the velocities v_i are given by

$$\partial_t r_1 + 6r_1 \partial_x r_1 = 0, \quad \partial_t r_2 + 2r_1 \partial_x r_2 = 0. \quad (25)$$

For solving these equations one can perform a classical hodograph transformation (see, e.g., [29]), that is, one assume that x and t are functions of the independent variables r_1 and r_2 : $t = t(r_1, r_2)$, $x = x(r_1, r_2)$. We find from Eqs. (25) that these functions must satisfy the linear system

$$\frac{\partial x}{\partial r_1} - 2r_1 \frac{\partial t}{\partial r_1} = 0, \quad \frac{\partial x}{\partial r_2} - 6r_1 \frac{\partial t}{\partial r_2} = 0.$$

At the boundary with the dispersionless solution [where $r_1 = r_R$, see (18a)] the first equation reads

$$\frac{\partial x_R}{\partial r_R} - 2r_R \frac{\partial t}{\partial r_R} = 0, \quad (26)$$

and this must be compatible with Eq. (24). Differentiation of Eq. (24) with respect to r_R and elimination of $\partial x_R / \partial r_R$ with the use of Eq. (26) yield the differential equation for the function $t(r_R) = t(r_R, 0)$:

$$4r_R \frac{dt}{dr_R} + 6t = -\frac{dw^A(r_R)}{dr_R}. \quad (27)$$

At the wave breaking time $r_{\text{R}} = 0$ and (27) gives the correct definition (8) of the wave breaking time: $t_{\text{WB}} = t(0)$. Elementary integration then yields

$$\begin{aligned} t(r_{\text{R}}) &= \frac{1}{4(-r_{\text{R}})^{3/2}} \int_0^{r_{\text{R}}} \sqrt{-r} \frac{dw^{\text{A}}(r)}{dr} dr \\ &= \frac{1}{8(-r_{\text{R}})^{3/2}} \int_0^{r_{\text{R}}} \frac{w^{\text{A}}(r)}{\sqrt{-r}} dr - \frac{w^{\text{A}}(r_{\text{R}})}{4r_{\text{R}}}. \end{aligned} \quad (28)$$

Substituting this expression into (24), we get the function $x_{\text{R}}(r_{\text{R}}) = x(r_{\text{R}}, 0)$,

$$\begin{aligned} x_{\text{R}}(r_{\text{R}}) &= -\frac{3}{2\sqrt{-r_{\text{R}}}} \int_0^{r_{\text{R}}} \sqrt{-r} \frac{dw^{\text{A}}(r)}{dr} dr + w^{\text{A}}(r_{\text{R}}) \\ &= -\frac{3}{4\sqrt{-r_{\text{R}}}} \int_0^{r_{\text{R}}} \frac{w^{\text{A}}(r)}{\sqrt{-r}} dr - \frac{1}{2} w^{\text{A}}(r_{\text{R}}). \end{aligned} \quad (29)$$

The two formulae (28) and (29) define in an implicit way the law of motion $x = x_{\text{R}}(t)$ of the soliton edge of the DSW.

The above expressions are correct as long as the soliton edge is located inside region A, that is up to the moment

$$t_{\text{A/B}} = t(-1) = \frac{1}{4} \int_0^{-1} \sqrt{-r} \frac{dw^{\text{A}}(r)}{dr} dr, \quad (30)$$

after which the soliton edge connects with region B. Concretely, for a time $t > t_{\text{A/B}}$, we have to solve the differential equation

$$4r_{\text{R}} \frac{dt}{dr_{\text{R}}} + 6t = -\frac{dw^{\text{B}}(r_{\text{R}})}{dr_{\text{R}}}$$

with the initial condition $t(-1) = t_{\text{A/B}}$. This yields

$$\begin{aligned} t(r_{\text{R}}) &= \frac{1}{4(-r_{\text{R}})^{3/2}} \left(\int_0^{-1} \sqrt{-r} \frac{dw^{\text{A}}(r)}{dr} dr \right. \\ &\quad \left. + \int_{-1}^{r_{\text{R}}} \sqrt{-r} \frac{dw^{\text{B}}(r)}{dr} dr \right), \end{aligned} \quad (31)$$

and

$$\begin{aligned} x_{\text{R}}(r_{\text{R}}) &= -\frac{3}{2(-r_{\text{R}})^{1/2}} \left(\int_0^{-1} \sqrt{-r} \frac{dw^{\text{A}}(r)}{dr} dr \right. \\ &\quad \left. + \int_{-1}^{r_{\text{R}}} \sqrt{-r} \frac{dw^{\text{B}}(r)}{dr} dr \right) + w^{\text{B}}(r_{\text{R}}). \end{aligned} \quad (32)$$

At asymptotically large time $t \rightarrow \infty$ one is at stage B of evolution with furthermore $r_{\text{R}} \rightarrow 0$. Hence the upper limit of integration in the second integrals of formulae (31) and (32) can be put equal to zero. Integration over r in the resulting expressions can be replaced by integration over x with account of the fact that $w^{\text{A,B}}(r)$ represent two branches of the inverse function of $r = u_0(x)$, so we get

$$t(r_{\text{R}}) \approx \frac{\mathcal{A}}{4(-r_{\text{R}})^{3/2}}, \quad \text{where} \quad \mathcal{A} = \int_{\mathbb{R}} \sqrt{-u_0(x)} dx$$

is a measure of the amplitude of the initial trough. Consequently,

$$r_{\text{R}}(t) = -\left(\frac{\mathcal{A}}{4t}\right)^{2/3}, \quad x_{\text{R}}(t) = -\frac{3\mathcal{A}^{2/3}}{2^{1/3}} t^{1/3}, \quad (33)$$

where we have neglected x_0 which is small compared with the infinitely increasing time-dependent terms.

At large time, the dispersionless part of the profile between $x = 0$ and $x_{\text{R}}(t)$ is stretched to a quasi-linear behavior $u(x, t) = x r_{\text{R}}(t)/x_{\text{R}}(t)$, and one thus has

$$\int_{x_{\text{R}}(t)}^0 dx \sqrt{-u(x, t)} = -\frac{2}{3} x_{\text{R}}(t) \sqrt{-r_{\text{R}}(t)} = \mathcal{A}, \quad (34)$$

which means that the quantity \mathcal{A} is conserved, at least at the level of the present asymptotic analysis. This situation is reminiscent of—but different from—the dissipative case where nonlinear patterns of triangular shape may also appear at the rear edge of a (viscous) shock. In the dissipative case also there exists a conserved quantity. For Burgers equation for instance, with an initial condition of type (6), a single viscous shock appears which is followed by an asymptotically triangular wave. This means that the details of the initial distribution are lost (as in the present case) but for Burgers equation the conserved quantity is $\int_{I(t)} dx u(x, t)$, where $I(t)$ is the support of the triangular wave (equivalent to our segment $[x_{\text{R}}(t), 0]$).

Formulae (33) suggest that in the vicinity of the soliton edge, the behavior of the DSW must be self-similar, and we now turn to the investigation of this possibility in the framework of Whitham theory.

IV. SIMILARITY SOLUTION AT THE SOLITON EDGE OF THE SHOCK

In this section we use the Whitham approach to obtain the long time asymptotic behavior of the shock close to $x_{\text{R}}(t)$, valid up to $x \sim -t^{1/3}(\ln t)^{3/2}$ (see Refs. [8, 9]).

Equations (33) suggest that, close to the soliton edge of the DSW, the Riemann invariants r_1 and r_2 have the following scaling form:

$$r_i = \frac{1}{t^{2/3}} R_i \left(\frac{x}{t^{1/3}} \right). \quad (35)$$

Here $x < 0$ and since $r_1 < r_2 < 0$, we have $R_1 < R_2 < 0$. The scaling (35) agrees with the scaling (3) of the full KdV equation first noticed in Refs. [4–6]. Written in terms of the re-scaled Riemann parameters R_1 and R_2 and of the self-similar variable $z = x/t^{1/3}$, the Whitham equations (11) read

$$\frac{dR_i}{dz} = -\frac{2R_i}{z - 3R_1 V_i(m)}, \quad i = 1, 2, \quad (36)$$

where

$$m = 1 - R_2/R_1, \quad (37)$$

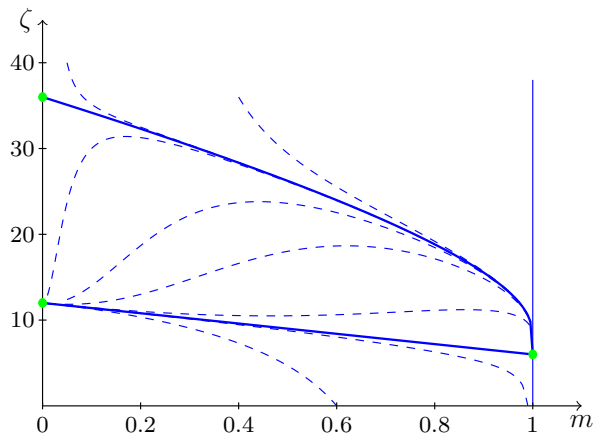


FIG. 3: Integral curves of Eq. (40). The separatrices are depicted as solid thick lines.

and the velocities $V_1(m)$ and $V_2(m)$ are given by

$$\begin{aligned} V_1(m) &= 2(2-m) - \frac{4mK(m)}{E(m) - K(m)}, \\ V_2(m) &= 2(2-m) + \frac{4m(1-m)K(m)}{E(m) - (1-m)K(m)}. \end{aligned} \quad (38)$$

The two equations (36) can be reduced to a single equation if we introduce the variable

$$\zeta = z/R_1 \quad (39)$$

and look for the dependence of ζ on m . Simple calculation yields the differential equation

$$\frac{d\zeta}{dm} = \frac{(\zeta - V_1(m))(\zeta - 3V_2(m))}{2(1-m)(V_2(m) - V_1(m))} \quad (40)$$

whose basic properties can be studied in the phase plane (m, ζ) . The phase portrait in this plane is displayed in Fig. 3. It has the singular points

$$\begin{array}{lll} (0, 12), & (0, 36) & \text{for } m = 0; \\ (1, 6), & (1, 6) & \text{for } m = 1, \end{array}$$

that is at $m = 1$ two singular points merge into one of a mixed type: for a part of the integral curves it is a saddle point and for the other part it is a source. Numerical solution of Eq. (40) suggests that the separatrix joining the singular points $(0, 12)$ and $(1, 6)$ is a straight line

$$\zeta = 6(2-m), \quad (41)$$

which, after returning to the variables R_1, R_2 and z leads to the assumption that the system (36) admits the following integral:

$$R_1 + R_2 = \frac{1}{6}z \quad (42)$$

A direct check shows that indeed $d(R_1 + R_2)/dz = 1/6$ under the condition (42), so that this assumption is proved. The integral curves beginning in vicinity of this separatrix are attracted to it when m decreases, so one can expect that just this separatrix realizes the self-similar regime of the DSW near its soliton edge.

To determine the dependence of m on z , we find, with the use of Eqs. (36),

$$\frac{dm}{dz} = \frac{6\zeta(m)(1-m)(V_2(m) - V_1(m))}{z[\zeta(m) - 3V_1(m)][\zeta(m) - 3V_2(m)]}. \quad (43)$$

Substituting Eq. (41) and the expressions (38) in the above, we get the following equation

$$\frac{dm}{dz} = -\frac{2-m}{zmK(m)}F(m), \quad (44)$$

where

$$F(m) = (2-m)E(m) - 2(1-m)K(m). \quad (45)$$

The solution of this equation determines $m = m(z)$ along the separatrix.

The form of expression (45) suggests that it can be obtained as a result of the calculation of some elliptic integral in which the integration limits may play the role of more convenient variables. Inspection of tables of such integrals shows that the formula 3.155.9 in Ref. [30] (which we write down here with notations slightly different from the original reference),

$$\begin{aligned} I &= 3 \int_{q_2}^{q_1} \sqrt{(q_1^2 - y^2)(y^2 - q_2^2)} dy \\ &= q_1 [(q_1^2 + q_2^2)E(m) - 2q_2^2K(m)], \end{aligned} \quad (46)$$

has a necessary structure. In Eq. (46) one has $q_1 > q_2 > 0$ and $m = 1 - (q_2/q_1)^2$.

To establish the link between the two expressions (45) and (46), it is enough to take

$$q_1^2 + q_2^2 = 1, \quad (47)$$

so that $1-m = q_2^2/q_1^2$, $2-m = 1/q_1^2$. Assuming that the variables q_1, q_2 satisfy (47), we obtain

$$q_1^2 = \frac{1}{2-m}, \quad q_2^2 = \frac{1-m}{2-m}, \quad (48)$$

and then, imposing $m = m$ we get $F(m) = (2-m)^{3/2}I$.

Since $dq_1/dm = q_1^3/2$, Eq. (44) can be cast under the form

$$\frac{dq_1}{d \ln(-z)} = -\frac{q_1}{2mK(m)}F(m), \quad (49)$$

which is more convenient for further calculations. On the other hand, the integral (46) with account of Eqs. (48) simplifies to

$$I = q_1[E(m) - 2(1-q_1^2)K(m)],$$

and its differentiation with respect to q_1 gives

$$\frac{dI}{dq_1} = 3q_1^2 m K(m). \quad (50)$$

With the help of the formulae obtained we transform Eq. (49) to

$$\frac{dI}{I} = -\frac{3}{2} d \ln(-z).$$

Then, integration of this equation with the boundary condition $z = z_1$ at $m = 1$ yields z as a function of m :

$$z = z_1 I^{-2/3}(m) = z_1 \frac{2-m}{F^{2/3}(m)} \quad (51)$$

where

$$z_1 = \frac{x_R(t)}{t^{1/3}} = -6(\mathcal{A}/4)^{2/3} \quad (52)$$

is the value of z for $m = 1$ (at the soliton edge of the DSW, see sec. III).

From the formulae $m = 1 - R_2/R_1$ and (48) we find the relationship between R_i and q_i :

$$R_1 = \frac{q_1^2}{6} z, \quad R_2 = \frac{q_2^2}{6} z, \quad (53)$$

so that for the dependence of the Riemann invariants on m we obtain

$$\begin{aligned} R_1(m) &= \frac{z_1}{6(2-m)I^{3/2}}, \\ R_2(m) &= \frac{(1-m)z_1}{6(2-m)I^{3/2}}. \end{aligned} \quad (54)$$

Formulae (51), (52) and (54), together with Eq. (35), completely determine the self-similar solution of the Whitham equations: for fixed t we have $x(m) = t^{1/3}z(m)$, so that all functions are defined parametrically, with m playing the role of the parameter. Up to notations, this solution coincides with the one obtained in Ref. [9] by means of the study of asymptotic Riemann-Hilbert problem.

In the harmonic limit $m \ll 1$, the relation (51) reads

$$m = m_1 z^{-3/4}, \quad \text{where} \quad m_1 = \frac{2^{11/4}}{\sqrt{3\pi}} (-z_1)^{3/4}, \quad (55)$$

which leads to the expressions

$$r_1 = \frac{x}{12t} - \frac{m_1}{24} \frac{(-x)^{1/4}}{t^{3/4}}, \quad r_2 = \frac{x}{12t} + \frac{m_1}{24} \frac{(-x)^{1/4}}{t^{3/4}}. \quad (56)$$

It is important to notice that the difference $r_2 - r_1$, that is, the amplitude of the oscillations in the ‘‘quasilinear’’ region of Zakharov and Manakov [7], increases with growing distance from the soliton edge [as $(-x)^{1/4}$], but $r_2/r_1 \rightarrow 1$ and $m \rightarrow 0$ here. Hence, this limit is not a small-amplitude one and therefore the self-similar regime cannot be realized along the whole DSW; it takes place close enough to the soliton edge only. Consequently, we have to turn to the general solution of the Whitham equations to obtain the full description of the DSW.

V. GENERAL SOLUTION

In this section, following Ref. [22], we turn to the general solution of the Whitham equations given by the formulae of Sec. II C. Our task now is to express the functions $W_i(r_1, r_2)$, $i = 1, 2$, in terms of the initial form $u_0(x)$ of the pulse. As was indicated above, at the first stage of evolution the DSW is located inside the region A and after the moment $t_{A/B}$ [see Eq. (30)] a second stage begins where it reaches region B. Correspondingly, the expressions for W_i and \mathscr{W} are given by different formulae and should be considered separately.

A. Solution in region A

In region A one can follow the procedure explained in Ref. [25]. One imposes the matching of the right edge of the DSW with the dispersionless solution (5): just at $x = x_R(t)$, we have $r_1 = r(x, t)$, where $r(x, t)$ is the solution of (4), and $v_1(r_1, 0) = 6r_1$ (this follows from Eq. (17)). Comparing in this case Eqs. (5) and (19) one obtains

$$W_1^A(r_1, 0) = w^A(r_1), \quad (57)$$

which embodies the same information as Eq. (18a). In terms of \mathscr{W} this corresponds to the equation

$$\mathscr{W}^A(r_1, 0) + 2r_1 \partial_1 \mathscr{W}^A(r_1, 0) = w^A(r_1), \quad (58)$$

whose solution is

$$\mathscr{W}^A(r_1, 0) = \frac{1}{2\sqrt{-r_1}} \int_{r_1}^0 \frac{w^A(\rho) d\rho}{\sqrt{-\rho}}. \quad (59)$$

This will serve as a boundary condition for the Euler-Poisson equation (22) whose general solution has been given by Eisenhart [32] in the form

$$\begin{aligned} \mathscr{W}^A(r_1, r_2) &= \int_{r_1}^0 \frac{\varphi^A(\mu) d\mu}{\sqrt{(\mu - r_1)|r_2 - \mu|}} + \\ &\int_{r_2}^0 \frac{\psi^A(\mu) d\mu}{\sqrt{(\mu - r_1)(\mu - r_2)}}, \end{aligned} \quad (60)$$

where the functions φ^A and ψ^A are arbitrary functions to be determined from the appropriate boundary conditions. By taking $r_2 = 0$ in this expression one sees that $\varphi^A(\mu)/\sqrt{-\mu}$ is the Abel transform of $\mathscr{W}^A(r_1, 0)$. The inverse transform reads [33]

$$\frac{\varphi^A(\mu)}{\sqrt{-\mu}} = -\frac{1}{\pi} \frac{d}{d\mu} \int_{\mu}^0 \frac{\mathscr{W}^A(r, 0) dr}{\sqrt{r - \mu}}. \quad (61)$$

Plugging expression (59) for $\mathscr{W}^A(r, 0)$ in this formula and changing the order of integration one obtains

$$\varphi^A(\mu) = \frac{1}{2\pi\sqrt{-\mu}} \int_{\mu}^0 \frac{w^A(\rho) d\rho}{\sqrt{\rho - \mu}}. \quad (62)$$

For the initial profile (6), w^A is given in Eq. (7) and one gets explicitly

$$\varphi^A(\mu) = -\frac{x_0}{4\pi} \left(3 + \frac{1+\mu}{\sqrt{-\mu}} \tanh^{-1} \sqrt{-\mu} \right).$$

In order to determine the function ψ^A , one considers the left boundary of the DSW where, according to (18b), r_1 and r_2 are asymptotically close to each other. Let us write $r_1 = r$ and $r_2 = r + \epsilon$ with $r \in [-1, 0]$ and ϵ small and positive. One gets from (60)

$$\begin{aligned} \mathscr{W}^A(r, r + \epsilon) &= \int_{r+\epsilon}^0 d\mu \frac{\varphi^A(\mu) + \psi^A(\mu)}{\sqrt{(\mu-r)(\mu-r-\epsilon)}} \\ &+ \int_r^{r+\epsilon} \frac{\varphi^A(\mu) d\mu}{\sqrt{(\mu-r)(r+\epsilon-\mu)}}. \end{aligned} \quad (63)$$

In the right hand side of the above equality, the second term converges when ϵ tends to 0 [towards $\pi\varphi^A(r)$], whereas the first one diverges unless $\varphi^A(r) + \psi^A(r) = 0$, this being true for all $r \in [-1, 0]$. This imposes that the functions φ^A and ψ^A should be opposite one the other and the final form of the Eisenhart solution in case A reads

$$\mathscr{W}^A(r_1, r_2) = \int_{r_1}^{r_2} \frac{\varphi^A(\mu) d\mu}{\sqrt{(\mu-r_1)(r_2-\mu)}}, \quad (64)$$

where φ^A is given by formula (62).

B. Solution in region B

One looks for a solution of the Euler-Poisson equation in region B of the form

$$\mathscr{W}^B(r_1, r_2) = \mathscr{W}^A(r_1, r_2) + \int_{-1}^{r_1} \frac{\varphi^B(\mu) d\mu}{\sqrt{(r_1-\mu)(r_2-\mu)}}. \quad (65)$$

Indeed, this ensures that \mathscr{W}^B , (i) being the sum of two solutions of the Euler-Poisson equation, is also a solution of this equation and (ii) verifies the boundary condition (23) since the second term of the right-hand side of (65) vanishes when $r_1 = -1$.

At the right boundary of the DSW, $\mathscr{W}^B(r_1, 0)$ verifies the same equation (58) as $\mathscr{W}^A(r_1, 0)$ does, where all the superscripts A should be replaced by B. The solution with the appropriate integration constant reads

$$\begin{aligned} \mathscr{W}^B(r_1, 0) &= \frac{1}{2\sqrt{-r_1}} \int_{r_1}^{-1} \frac{w^B(\rho) d\rho}{\sqrt{-\rho}} \\ &+ \frac{1}{2\sqrt{-r_1}} \int_{-1}^0 \frac{w^A(\rho) d\rho}{\sqrt{-\rho}}. \end{aligned} \quad (66)$$

The same procedure than the one previously used in part A of the DSW leads here to

$$\varphi^B(\mu) = \frac{1}{2\pi\sqrt{-\mu}} \int_{-1}^{\mu} d\rho \frac{w^A(\rho) - w^B(\rho)}{\sqrt{\mu-\rho}}. \quad (67)$$

For the initial profile (6) one gets explicitly

$$\varphi^B(\mu) = -\frac{x_0}{4} \frac{1+\mu}{\sqrt{-\mu}}.$$

In the generic case, Eqs. (65) and (67) give the solution of the Euler-Poisson equation in region B.

C. Characteristics of the DSW at its edges

It is important to determine the boundaries $x_R(t)$ and $x_L(t)$ of the DSW, as well as the values of the Riemann invariants r_1 and r_2 at these points. The law of motion of the soliton edge was already found in Sec. III and it is instructive to show how this result can be obtained from the general solution.

At the soliton edge we have $r_2 = r_3 = 0$ and $r_1 = r_R(t)$. The corresponding Whitham velocities are $v_1 = 6r_R$ and $v_2 = 2r_R$ [see Eqs. (17)], and the two equations (19) read

$$\begin{aligned} x_R - 6r_R t &= W_1(r_R, 0) = w(r_R), \\ x_R - 2r_R t &= W_2(r_R, 0) = \mathscr{W}(r_R, 0). \end{aligned} \quad (68)$$

These formulae apply to both stages of evolution and therefore the superscripts A and B are dropped out. They give at once

$$\begin{aligned} t(r_R) &= \frac{1}{4r_R} [\mathscr{W}(r_R, 0) - w(r_R)], \\ x_R(r_R) &= \frac{1}{2} [3\mathscr{W}(r_R, 0) - w(r_R)]. \end{aligned} \quad (69)$$

Let us consider the stage A for instance. Eq. (59) yields

$$\mathscr{W}^A(r_R, 0) = -\frac{1}{2\sqrt{r_R}} \int_0^{r_R} \frac{w^A(\rho) d\rho}{\sqrt{-\rho}},$$

which, inserted into Eqs. (69) gives immediately the results (28) and (29). For instance, for the initial profile (6), when the right boundary is still in region A, one obtains explicitly

$$t(r_R) = \frac{x_0}{16r_R} \left(\sqrt{1+r_R} - \frac{\arcsin \sqrt{-r_R}}{\sqrt{-r_R}} \right). \quad (70)$$

At the wave breaking time $r_R = 0$ and this yields $t_{\text{WB}} = t(r_R = 0) = x_0/24$ as already obtained [cf. Eq. (8)]. Stage A ends at time $t_{A/B}$ at which the minimum (-1) of the smooth part of the profile enters the DSW. This corresponds to $t_{A/B} = t(r_R = -1)$ and yields, for the initial parabolic profile (6): $t_{A/B} = \pi x_0/32$.

Let us now turn to the determination of the location $x_L(t)$ of the left boundary of the DSW, and of the common value $r_L(t)$ of r_1 and r_2 at this point. In the typical situation the left boundary is located in region A. In this case the equations (19) for $i = 1$ and 2 are equivalent and read

$$x_L - 12r_L \cdot t = W_1^A(r_L, r_L). \quad (71)$$

An equation for r_L alone is obtained by demanding that the velocity dx_L/dt of the left boundary is equal to the common value $12r_L$ of v_1 and v_2 at this point [cf. Eqs. (15)]. The time derivative of Eq. (71) then yields

$$t = -\frac{1}{12} \frac{dW_1^A(r_L, r_L)}{dr_L}. \quad (72)$$

Once $r_L(t)$ has been determined by solving this equation, $x_L(t)$ is given by Eq. (71).

Note that the relation $dx_L/dt = 12r_L$ is a consequence of the general statement that the small amplitude edge of the DSW propagates with the group velocity corresponding to the wave number determined by the solution of the Whitham equations. Indeed, the KdV group velocity of a linear wave with wave-vector k moving over a zero background is $v_g = -3k^2$, and here $k = 2\pi/L = 2\sqrt{-r_L}$ [cf. Eq. (10)], hence $v_g = 12r_L = dx_L/dt$, as it should be. This property of the small-amplitude edge is especially important in the theory of DSWs for non-integrable equations (see [34, 35]).

We also study below a case different from (6) for which the left boundary of the DSW belongs to region B and corresponds to $r_1 = r_2 = -1$ [in the so-called triangular case corresponding to $u_0(x)$ given by Eq. (74)]. Then, at the small amplitude edge $v_1 = v_2 = -12$ and Eqs. (19) yield $x_L + 12 \cdot t = C^{\text{st}}$, the constant being the common value of $W_1^{\text{p}}(-1, -1)$ and $W_2^{\text{p}}(-1, -1)$. It can be determined at $t = t_{\text{WB}}$, leading in this case to

$$x_L = -x_0 - 12(t - t_{\text{WB}}). \quad (73)$$

It is worth noticing that the velocity $dx_L/dt = -12$ agrees with the leading term in Eq. (56) for $r_1 = -1$ in spite of a non-vanishing amplitude of the self-similar solution in this limit. For a more detailed study of the small-amplitude region beyond the Whitham approximation see, e.g., Ref. [12].

D. The global picture

We now compare the results of the Whitham approach with the numerical solution of the KdV equation for the initial profile (6) and also for a profile

$$u_0(x) = \begin{cases} -1 + \left| \frac{2x}{x_0} + 1 \right| & \text{for } -x_0 \leq x \leq 0, \\ 0 & \text{elsewhere.} \end{cases} \quad (74)$$

This profile is represented in Fig. 4 at $t = 0$, at wave-breaking time $t = t_{\text{WB}}$, which in the present case is equal to $t_{\text{WB}} = x_0/12$, and also at $t = 2t_{\text{WB}}$ (in the dispersionless approximation).

We henceforth denote the initial profile (6) as “parabolic” and the initial profile (74) as “triangular”. As was indicated above, the triangular profile has the particularity of having a DSW within the region B only. This is clear from Fig. 4: part A of the initial profile does not penetrate into the DSW region before part B does.

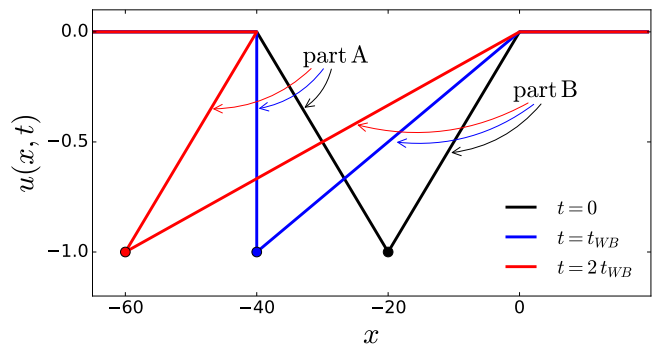


FIG. 4: Dispersionless evolution of the initial triangular profile (74) with $x_0 = 40$. The black, blue and red solid lines represent $r(x, t)$ solution of (4) for times $t = 0$, $t = t_{\text{WB}}$ and $t = 2t_{\text{WB}}$.

Or, phrasing this differently: according to the dispersionless evolution, at $t = t_{\text{WB}}$ both parts A and B penetrate into the region of multi-valuedness at $x \leq x_0$.

The DSW is described by Whitham method as explained in Sections II B and II C. For this purpose one needs to determine r_1 and r_2 as functions of x and t ($r_3 \equiv 0$). This is performed as follows:

- First, we pick up a given $r_1 \in [-1, r_R]$, where r_R is the value of r_1 at the soliton edge, the point where the DSW is connected to the rarefaction wave (it has been explained in Sec. V C how to compute it).
- Second, at fixed t and r_1 , we find the corresponding value r_2 as a solution of the difference equation obtained from Eqs. (19)

$$(v_1 - v_2) \cdot t = W_2(r_1, r_2) - W_1(r_1, r_2), \quad (75)$$

where W_1 and W_2 are computed from Eq. (21).

- Last, the corresponding value of x is determined by $x = W_1 + v_1 t$ (or equivalently $x = W_2 + v_2 t$).

This procedure gives, for each $r_1 \in [-1, r_R]$ and t , the value of r_2 and x . In practice, it makes it possible to associate to each (x, t) a couple (r_1, r_2) . The result is shown in Figs. 5 for the two initial profiles (6) and (74).

Note that the characteristics of the DSW are different for the initial profiles (6) and (74): for the parabolic profile, in the upper left plot of Fig. 5, the edge point of the DSW—at (x_0, t_{WB}) —pertains to region A and corresponds to $r_1 = 0$, while for the triangular profile, in the lower left plot of Fig. 5, the edge point of the DSW belongs to region B, with $r_1 = -1$. For the parabolic profile, the value $r_1 = -1$ defines a line which separates the regions A and B of the plane (x, t) (see the upper left plot of Fig. 5). This line reaches a boundary of the DSW only at $x_R(t_{A/B})$, where $t_{A/B}$ is the time where part A of the initial profile has just been completely absorbed within the DSW. On the other hand, for the triangular

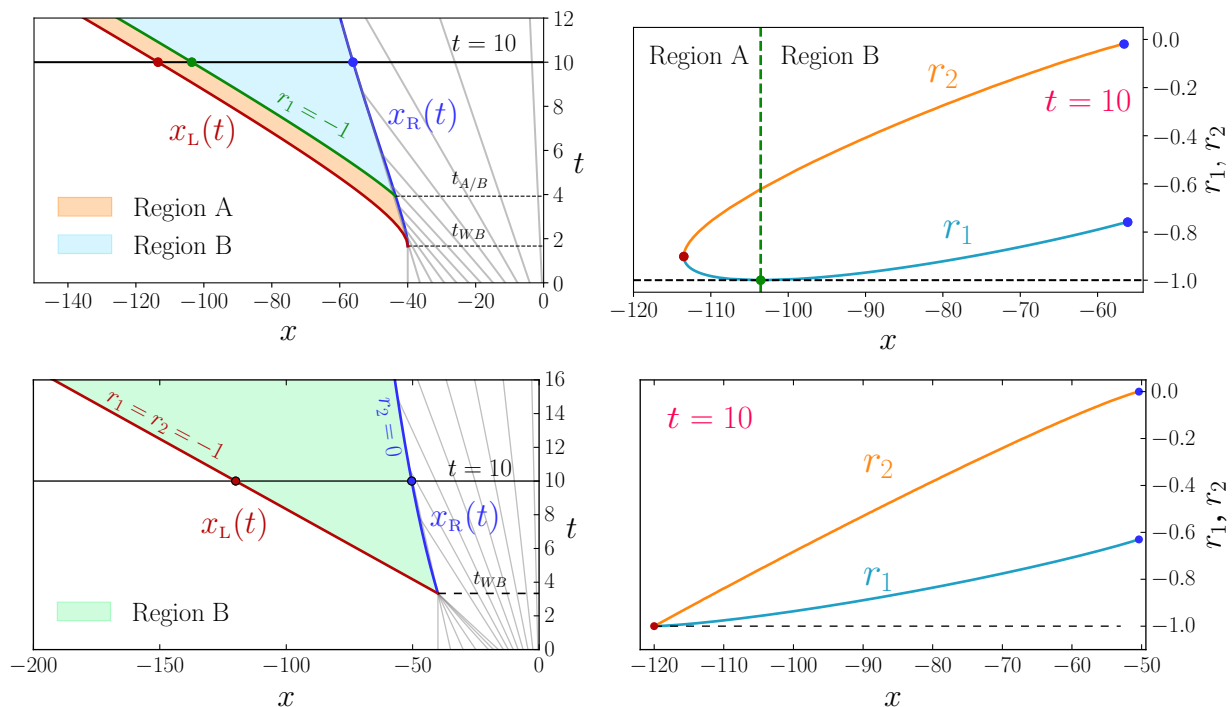


FIG. 5: The lower plots refer to the triangular initial profile, and the upper ones to the parabolic initial profile. Left column: different regions in the (x, t) plane. The DSW occurs in the colored regions. The characteristics of the dispersionless evolution are represented as gray lines. In the upper left plot the time $t_{A/B}$ is the time where part A of the initial profile has been completely absorbed by the DSW. For the triangular profile $t_{A/B} = t_{WB}$. Right column: plot of the two varying Riemann invariants r_1 and r_2 at fixed $t = 10$ for $x_L(t) \leq x \leq x_R(t)$.

profile, the whole left boundary of the DSW corresponds to the line $r_1 = -1$ (see the lower left plot of Fig. 5).

The knowledge of $r_1(x, t)$ and $r_2(x, t)$ makes it possible to determine, for each time $t > t_{WB}$, $u(x, t)$ as given by the Whitham approach, for all $x \in \mathbb{R}$:

- (i) In the regions $x \geq 0$ and $x \leq x_L(t)$, we have $u(x, t) = 0$.
- (ii) In the region $[x_R(t), 0]$ $u(x, t) = r(x, t)$ which is solution of the Hopf equation (obtained by the method of characteristics).
- (iii) Inside the DSW, for $x \in [x_L(t), x_R(t)]$, the function $u(x, t)$ is given by the expression (9), with $r_3 = 0$ and r_1 and r_2 determined as functions of x and t by the procedure just explained.

The corresponding profiles are shown in Fig. 6 for the parabolic and triangular initial distributions. The agreement with the numerical simulation is excellent in both cases.

In Fig. 7 we also compare the wave-length of the non-linear oscillations within the DSW as determined by Whitham approach [Eq. (10)] with the results of numerical simulations, and the agreement is again very good.

E. The initial square profile

In this section we discuss another type of initial condition, which we denote as “square profile”:

$$u_0(x) = \begin{cases} -1 & \text{for } -x_0 \leq x \leq 0, \\ 0 & \text{elsewhere.} \end{cases} \quad (76)$$

El and Grimshaw already theoretically studied the same initial condition by using the method just exposed [36]. We will here compare the theory with numerical simulations to indicate some limitations of the one-phase Whitham method which we use in the present work.

For this initial profile, wave breaking occurs instantaneously, and until $t \leq x_0/4$ a plateau (i.e., a segment with constant $u(x, t) = -1$) separates the DSW (at the right) from a rarefaction wave (at the left). In this configuration, the DSW corresponds to the standard Gurevich-Pitaevskii scheme for a step-like initial profile with a single varying Riemann invariant (r_2 in this case). This DSW can be described using the self-similar variable $\zeta = (x + x_0)/t$, in this case Eq. (11) for $i = 2$ reads $\zeta = v_2(-1, r_2)$. One also obtains $x_L(t) = -x_0 - 2t$, $x_R(t) = -6t$ and the rarefaction wave corresponds to $r(x, t) = x/6t$ for $x \in [x_R(t), 0]$.

It is interesting to remark that the Gurevich-Pitaevskii DSW can also be described within the approach exposed

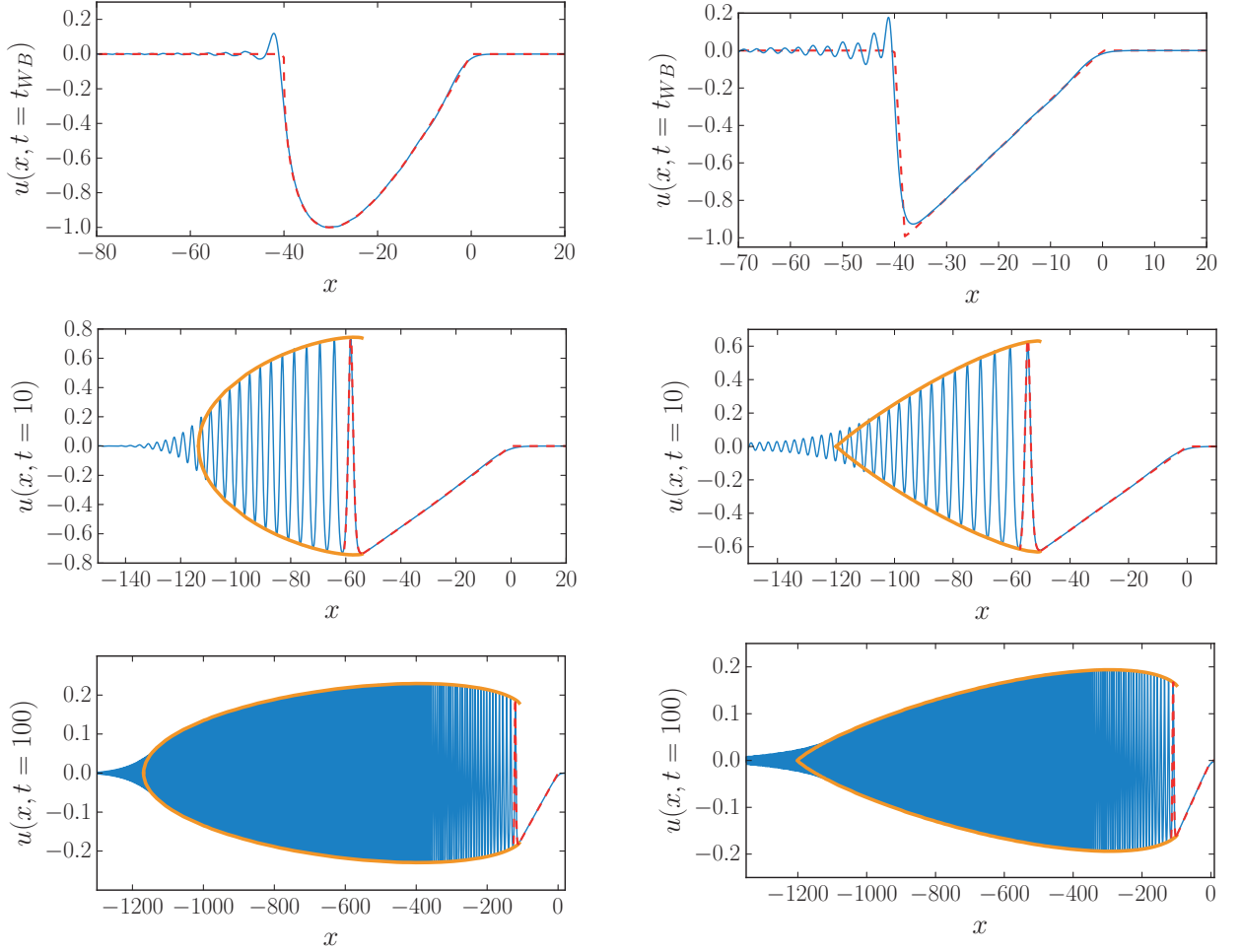


FIG. 6: $u(x, t)$ as a function of x for fixed t . The upper row corresponds to the wave-breaking time t_{WB} , the central row to $t = 10$ and the lower one to $t = 100$. The left column refers to the parabolic initial profile, and the right one to the triangular initial profile. The blue solid line corresponds to the numerical solution of Eq. (2). The envelopes correspond to the results of Whitham modulation theory. The dashed red lines represent the dispersionless profile $r(x, t)$ and also (in the two lower rows) the Whitham result for the soliton at the large amplitude boundary of the DSW.

in Secs. II C and V D, by solving Eq. (19) for $i = 2$. Here W_2^A should be computed from

$$\mathcal{W}^A(r_1, r_2) = -x_0 \quad (77)$$

by means of Eq. (21). The form (77) of \mathcal{W}^A comes from (64) with $w^A(r) = -x_0$.

At $t = x_0/4$ the plateau disappears, and one enters in region B with two varying Riemann invariants. Formulae (65) and (67) lead here to

$$\begin{aligned} \mathcal{W}^B(r_1, r_2) &= -x_0 - \frac{x_0}{\pi} \int_{-1}^{r_1} \frac{\sqrt{\mu+1} d\mu}{\sqrt{-\mu(r_1-\mu)(r_2-\mu)}}, \\ &= -x_0 + \frac{2x_0/\pi}{\sqrt{-r_1(1+r_2)}} \times \\ &\quad \times \left\{ \Pi\left(\frac{1+r_1}{r_1}, m\right) - K(m) \right\}, \end{aligned} \quad (78)$$

where $m = (1 + 1/r_1)/(1 + 1/r_2)$ and Π is the complete elliptic integral of the third kind.

The predictions of Whitham theory are compared in Fig. 8 with numerical simulations. Surprisingly enough, the agreement between simulation and theory decreases at large time: at $t = 100$ one can notice oscillations in the envelope of the front part of the DSW (Gurevich-Pitaevskii part). Inspection of the dynamics of formation of the nonlinear structure reveals that, during the formation of the rear rarefaction wave, some oscillations appear due to dispersive effects associated with the discontinuity of the initial condition (76): their interference with the oscillations of the DSW leads to the modulated structure which can be observed in the lower plot of Fig. 8. Such a behavior requires a two-phase approach for a correct description. Note also that for numerical purposes the initial condition is smoothed [39] and that the beating phenomenon increases for sharper initial condition (or a

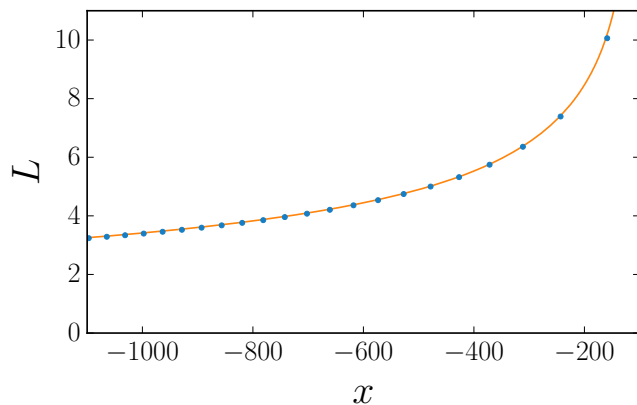


FIG. 7: Evolution of the wavelength of the nonlinear oscillations within the DSW as a function of position x . The figure corresponds to the time evolution of the parabolic initial profile represented in the lower left plot of Fig. 6 ($t = 100$). The continuous line represents the results of Whitham theory and the points are the value of the wavelength extracted from the numerical simulations.

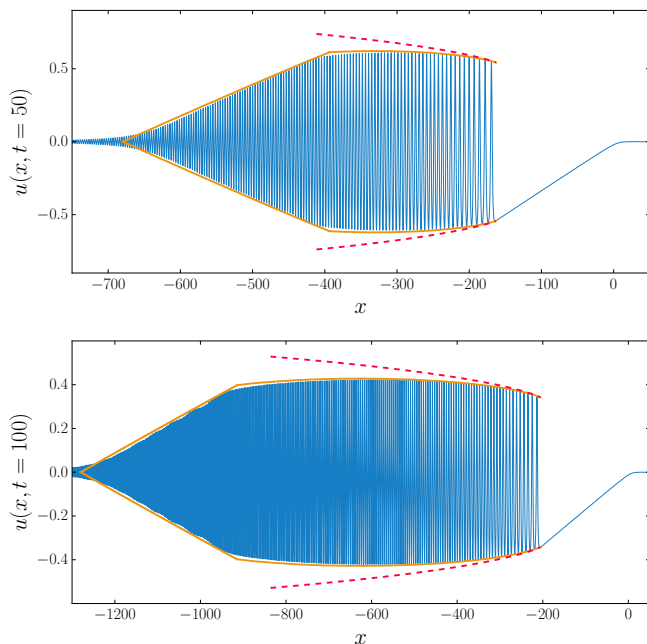


FIG. 8: Evolution of an initial square profile of type (76) with $x_0 = 80$ after a time $t = 50$ (upper plot) and $t = 100$ (lower plot). The blue solid lines are the results of numerical simulations. The orange envelopes are determined by Whitham method. The red dashed envelopes are the asymptotic self-similar results obtained in Sec. IV. Note the change of scale in the axis of the two plots.

lower values of x_0).

The predictions of the self-similar solution of Sec. IV are also displayed in Fig. 8. In this figure, the envelopes of the DSW expected from Eqs. (35) and (54) are represented by red dashed lines. In the vicinity of its soliton edge, the DSW is accurately described by the similarity solution. However this approach is not able to tackle the other, small amplitude, boundary of the shock. This is expected since —as discussed above— in the small amplitude region a scaling different from the one of Eq. (3) holds, with the relevant self-similar parameter $\zeta = (x + x_0)/t$; see Refs. [9, 37] for a general discussion.

VI. CONCLUSION

In the present work we have studied asymptotic solutions of the KdV equation for which no soliton is formed in the limit $t \rightarrow \infty$. We used the Whitham modulation theory combined with the generalized hodograph method for describing the DSW which is formed after wave breaking. A simple similarity description has been also obtained near the large amplitude region of the shock, still within the framework of Whitham's approach. Our results confirm, simplify and extend in some respects the previous works on this subject. We show that this theory provides a practical tool for the description of nonlinear evolution of pulses and can be used for comparison with experimental data. Besides that, it yields simple enough analytic formulae for some characteristic features of DSWs and reveals different scaling regimes of DSW evolution. Extensions of this approach to non completely integrable equations [35] and to other systems of physical interest are under study.

Acknowledgments

A. M. K. thanks Laboratoire de Physique Théorique et Modèles Statistiques (Université Paris-Saclay) where this work was started, for kind hospitality. This work was supported by the French ANR under Grant No. ANR-15-CE30-0017 (Haralab project).

-
- [1] G. B. Whitham, *Linear and Nonlinear Waves* (Wiley Interscience, New York, 1974).
 [2] V. I. Karpman, *Phys. Lett. A* **25**, 708 (1967),

doi:10.1016/0375-9601(67)90953-X.

- [3] C. S. Gardner, J. M. Green, M. D. Kruskal, and R. M. Miura, *Phys. Rev. Lett.* **19**, 1095 (1967),

- doi:10.1103/PhysRevLett.19.1095.
- [4] I. A. Berezin and V. I. Karpman, Zh. Eksp. Teor. Fiz. **46**, 1880 (1964) [Sov. Phys. JETP **19**, 1265 (1964)].
- [5] A. B. Shabat, Doklady AN SSSR **211**, 1310 (1973) [Sov. Mathem. Dokl. **14**, 1266 (1973)].
- [6] M. J. Ablowitz and A. C. Newell, J. Math. Phys. **14**, 1277 (1973), doi:10.1063/1.1666479.
- [7] V. E. Zakharov and S. V. Manakov, Zh. Eksp. Teor. Fiz. **71**, 203 (1976) [Sov. Phys. JETP, **44**, 106 (1976)].
- [8] M. J. Ablowitz and H. Segur, Stud. Appl. Math. **57**, 13 (1977), doi:10.1002/sapm197757113.
- [9] P. Deift, S. Venakides, and Z. Zhou, Commun. Pure Appl. Math. **47**, 199 (1994), doi:10.1002/cpa.3160470204.
- [10] G. A. El, A. L. Krylov, and S. Venakides, Commun. Pure Appl. Math. **54**, 1243 (2001), doi:10.1002/cpa.10002.
- [11] T. Claeys and T. Grava, Commun. Math. Phys. **286**, 979 (2009), doi:10.1007/s00220-008-0680-5.
- [12] T. Claeys and T. Grava, Commun. Pure Appl. Math. **63**, 203 (2010), doi:10.1002/cpa.20277.
- [13] J. L. Hammack and H. Segur, J. Fluid Mech. **65**, 289 (1974) doi:10.1017/S002211207400139X; *ibid.*, J. Fluid Mech. **84**, 337 (1978) doi:10.1017/S0022112078000208.
- [14] S. Trillo, M. Klein, G. F. Clauss, M. Onorato, Physica D **333**, 276 (2016) doi:10.1016/j.physd.2016.01.007.
- [15] A. M. Kamchatnov, A. Gammal, R. A. Kraenkel, Phys. Rev. A **69**, 063605 (2004) doi:10.1103/PhysRevA.69.063605.
- [16] M. A. Hoefer, M. J. Ablowitz, I. Coddington, E. A. Cornell, P. Engels, and V. Schweikhard, Phys. Rev. A **74**, 023623 (2006), doi:10.1103/PhysRevA.74.023623.
- [17] W. Wan, S. Jia, and J. W. Fleischer, Nature Phys. **3**, 46 (2007), doi:10.1038/nphys486.
- [18] G. Xu, M. Conforti, A. Kudlinski, A. Mussot, and S. Trillo, Phys. Rev. Lett. **118**, 254101 (2017), doi:10.1103/PhysRevLett.118.254101.
- [19] G. B. Whitham, Proc. R. Soc. A **283**, 238 (1965), doi:10.1098/rspa.1965.0019.
- [20] A. V. Gurevich and L. P. Pitaevskii, Zh. Eksp. Teor. Fiz. **65**, 590 (1973) [Sov. Phys. JETP **38**, 291 (1974)].
- [21] G. A. El and M. A. Hoefer, Physica D **333**, 11 (2016), doi:10.1016/j.physd.2016.04.006
- [22] G. A. El and V. V. Khodorovsky, Phys. Lett. A **182**, 49 (1993), doi:10.1016/0375-9601(93)90051-Z.
- [23] A. V. Gurevich, A. L. Krylov, and N. G. Mazur, Zh. Eksp. Teor. Fiz. **95**, 1674 (1989) [Sov. Phys. JETP **68**, 966 (1989)].
- [24] A. V. Gurevich, A. L. Krylov and G. A. El, Pis'ma Zh. Eksp. Teor. Fiz. **54**, 104 (1991) [JETP Lett. **54**, 102 (1991)].
- [25] A. V. Gurevich, A. L. Krylov and G. A. El, Zh. Eksp. Teor. Fiz. **101**, 1797 (1992) [Sov. Phys. JETP **74**, 957 (1992)].
- [26] A. L. Krylov, V. V. Khodorovskii and G. A. El, Pis'ma Zh. Eksp. Teor. Fiz. **56**, 325 (1992) [JETP Lett. **56**, 323 (1992)].
- [27] O. C. Wright, Commun. Pure Appl. Math. **46**, 423 (1993) doi:10.1002/cpa.3160460306
- [28] F. R. Tian, Commun. Pure Appl. Math. **46**, 1093 (1993) doi:10.1002/cpa.3160460802.
- [29] A. M. Kamchatnov, *Nonlinear Periodic Waves and Their Modulations—An Introductory Course*, (World Scientific, Singapore, 2000).
- [30] I. S. Gradshteyn and I. M. Ryzhik, Table of Integrals, Series, and Products, (Academic Press, New York, 1966).
- [31] S. P. Tsarev, Math. USSR Izv. **37**, 397 (1991), doi:10.1070/IM1991v037n02ABEH002069.
- [32] L. P. Eisenhart, Ann. Math. **120**, 262 (1918).
- [33] G. Arfken and H. J. Weber, *Mathematical Methods for Physicists* (Academic Press, Orlando, 2005).
- [34] G. A. El, Chaos **15**, 037103 (2005), doi:10.1063/1.1947120; *ibid.* **16**, 029901 (2006), doi:10.1063/1.2186766.
- [35] A. M. Kamchatnov, “On the dispersive shock waves theory for non-integrable equations”, <http://arxiv.org/abs/1809.08553>
- [36] G. A. El and R. H. J. Grimshaw, Chaos **12**, 1015 (2002), doi:10.1063/1.1507381.
- [37] H. Segur and M. J. Ablowitz, Physica D **3**, 165 (1981) doi:10.1016/0167-2789(81)90124-X
- [38] A so-called N -wave appears if $u_0(x)$ has both polarities.
- [39] In the numerical simulations presented in Fig. 8 we take $u_0(x) = \frac{1}{4}(\tanh(x/\Delta) - 1) \times (1 + \tanh((x+x_0)/\Delta))$ with $\Delta = 2$. This profile tends to (76) when $\Delta \rightarrow 0$.